REDUCTION OF STRUCTURAL DAMAGE BY NONLINEAR SOIL RESPONSE

By M. D. Trifunac[1] and M. I. Todorovska,[2] Members, ASCE

ABSTRACT: Following the 1994 Northridge earthquake, the areas with a high density of reported breaks in water pipes in typical residential areas in San Fernando Valley and in Los Angeles often did not coincide with the areas having a high density of severely damaged (red-tagged) buildings. As the former is an indicator of large strains and nonlinear soil response, this observation suggests that the damage to buildings in some areas may have been smaller than expected because the soil dissipated part of the energy of the ground motion by nonlinear response. This paper presents an attempt to quantify this relationship between the density of red-tagged buildings, N (per km^2), and the severity of shaking (via peak horizontal ground velocity, $v_{\max}$, or modified Mercalli intensity, I_{MM}), including the density of breaks in water pipes, n (per km^2), as a variable specifying the level of strain in the soil. Approximate empirical relationships for $N = f(v_{\max}, n)$ and $N = f(I_{MM}, n)$ are presented. The trends in the data indicate that, for $v_{\max}$ in the range from $\sim$35 to $\sim$125 cm/s, the rate of growth of N versus $v_{\max}$ tends to decrease at sites with large strain in the soil (i.e., large n). For $v_{\max}$ beyond $\sim$150 cm/s, the beneficial effects of nonlinear soil response seem to fade out, as large differential motions associated with soil failure begin to contribute to the damage of structures. Assuming fairly uniform density and quality of building stock and of water pipes in the areas studied, the derived relationships are then used to map $v_{\max}$ and I_{MM} in San Fernando Valley and in Los Angeles. The resulting maps are more detailed than what could be obtained from the density of strong motion stations and of sites with reports on felt intensity.

INTRODUCTION

The Northridge, California, earthquake of January 17, 1994, (M_L = 6.4) occurred on a blind thrust fault under the densely populated San Fernando Valley (northwestern region of the Los Angeles metropolitan area) (Wald et al. 1996) and caused the costliest natural disaster in the United States. Field surveys of the damage to man-made structures and ground failure (e.g., liquefaction, lateral spreading, dynamic settlement, and landslides) were conducted, and the data are being studied to assess the vulnerability of the metropolitan area to future severe earthquake shaking (EERI 1996; Stewart et al. 1994; Harp and Jibson 1996). Ground motion was recorded by more than 200 stations of four strong motion networks (operated by the U.S. Geological Survey, the University of Southern California, the California Division of Mines and Geology, and the Los Angeles Department of Water and Power) (EERI 1994, 1996; Trifunac et al. 1994, 1996). By the total number, density, and location of recording stations (relative to the causative fault), this has been by far the best recorded earthquake, and it was possible to draw smoothed contour maps of peak amplitudes and response spectrum amplitudes of ground motion (Trifunac et al. 1994, 1996; Todorovska and Trifunac 1997a,b). Smoothed contour maps of modified Mercalli intensity were prepared based on felt reports of the shaking at selected locations (Dewey et al. 1994). However, neither the density of strong motion stations nor the density of sites used by Dewey et al. (1994) were sufficient to help in interpretation of the concentrated patterns and spatial fluctuations of observed strong motion effects (Gao et al. 1996; Spudich et al. 1996) and of the observed damage (Stewart et al. 1994). The smoothed contour maps could be used to find only the average overall trends of the degree of damage as a function of the level of ground shaking (Trifunac and Todorovska 1997a,b). Recorded strong ground motion was also used to search for indicators of nonlinear soil response, based on reduction of peak ground acceleration at ''soft'' soil sites, relative to ''hard'' soil sites (Trifunac and Todorovska 1996).

Long before the age of digital computers and strong motion instruments, variations of strong motion amplitudes were studied via the distribution of damaged buildings (Kanai 1983). In San Fernando Valley, the relative similarity of structural types and construction materials used in residential houses as well as the fairly uniform density of houses and large areas covered by residential buildings make it possible to use the distribution of damaged buildings to infer approximately the associated levels of shaking. Similarly, if water pipes are assumed to be uniformly distributed in typical residential areas, the distribution of reported breaks can help to estimate the strain and whether nonlinear soil response occurred. Well-calibrated empirical scaling functions describing damage to buildings and water pipelines in terms of ground motion characteristics may be used to predict statistically the percentage of buildings and water lines that will be damaged during future earthquakes. Vice versa, one can estimate (roughly) certain ground motion characteristics in areas where there are no instrumental records by using the inverse of the above scaling equations. Such relationships were presented by Trifunac and Todorovska (1997a,b) for the number of red-tagged buildings per km^2, N (mostly wood-frame structures), and for the number of breaks in water pipes per km^2, n, based on damage and ground motion data in typical residential neighborhoods of San Fernando Valley and Los Angeles, following the Northridge earthquake. They used data on tagged buildings and breaks in water pipes (gathered by City of Los Angeles Department of Building Safety and Department of Water and Power) (Stewart et al. 1994), smoothed contour maps of horizontal peak ground velocity and peak strain factors presented by Trifunac et al. (1996) and a modified Mercalli intensity map prepared by Dewey et al. (1994). Trifunac and Todorovska (1997a,b) analyzed the data sets on red-tagged buildings and on breaks in water pipes independently of each other. Their results, based on actual data, are an improvement over damage curves based on expert opinion, but are specific for the prevailing geologic and soil conditions for these two regions, and for the prevailing type and density of buildings there (Wood Frame Construction, typical of the post–World War II period).

This study was motivated by and represents an extension of the work of Trifunac and Todorovska (1997a,b). A procedure similar to theirs is used to establish empirical scaling functions

[1]Prof., Dept. of Civ. Engrg., Univ. of Southern California, Los Angeles, CA 90089-2531.

[2]Res. Assoc. Prof., Dept. of Civ. Engrg., Univ. of Southern California, Los Angeles, CA.

Note. Associate Editor: Chia-Ming Uang. Discussion open until June 1, 1999. To extend the closing date one month, a written request must be filed with the ASCE Manager of Journals. The manuscript for this paper was submitted for review and possible publication on September 9, 1996. This paper is part of the ***Journal of Structural Engineering***, Vol. 125, No. 1, January, 1999. ©ASCE, ISSN 0733-9445/99/0001-0089–0097/$8.00 + $.50 per page. Paper No. 14069.

for the number of red-tagged buildings per km^2, N, as a function of the density of breaks in water pipes, n (as a measure of strain in the soil), and the peak horizontal ground velocity, $v_{\max}$, or intensity of shaking, I_{MM}. The motivation for including n in scaling of N results from an observation that, following the Northridge earthquake, the areas with high density of red-tagged (severely damaged) buildings and the areas with high density of pipe breaks are often disjointed (this is discussed in more detail in the next section). One explanation is that the soil, responding in a nonlinear manner, absorbed a portion of the incoming wave energy resulting in reduced damage to the buildings (Trifunac and Todorovska 1998a,b). The aim of this paper is to analyze this effect quantitatively. Next, the established empirical scaling functions $N = f(v_{\max}, n)$ and $N = f(I_{MM}, n)$ are inverted to evaluate $v_{\max}$ and I_{MM}, given N and n. The results are then used to map the spatial variations of $v_{\max}$ and I_{MM} in San Fernando Valley and in Los Angeles during the Northridge earthquake. The variations of $v_{\max}$ and I_{MM}, seen in these maps, are then discussed, with emphasis on the size of areas with very strong and very weak ground motion, the needed density of strong motion stations to capture such variations, the degree to which such variations are likely to be repeated during future earthquakes, and whether such variations can be predicted within the framework of probabilistic seismic hazard analyses.

OBSERVED DAMAGE AND GROUND MOTION

The study areas of Trifunac and Todorovska (1997a,b), and also of this paper, are typical residential neighborhoods of the San Fernando Valley and Los Angeles regions, shown by rectangles in Fig. 1. The areas with residential neighborhoods are outlined by the heavy irregular lines. The circular, triangular, rectangular, and diamond symbols indicate locations where strong ground motion was recorded (stations operated by University of Southern California, California Division of Mines and Geology, U.S. Geological Survey, and Los Angeles Department of Water and Power, respectively). Enlarged full and open symbols indicate, respectively, reduction (possibly due to nonlinear soil response) and amplification of horizontal peak acceleration relative to the average trend on ''hard'' soil sites, determined from nonparametric attenuation functions specific for this earthquake (Trifunac and Todorovska 1996; 1998a,b).

Fig. 2 shows the two regions in relation to the causative fault and the sites where major damage occurred (EERI 1994). The dotted line outlines the surface projection of the aftershock area. The small triangular, diamond, circular, and square symbols show the locations of the strong motion stations. The shaded regions outlined by heavy solid lines indicate zones of concentrated ground breakage (EERI 1994). Other sites of interest are shown by capital letters: A—Simi Valley Tailings Dam; B—Jensen Filtration Plant; C—San Fernando Valley Juvenile Hall; D—Pacoima Dam Site; and E—intersection of Mulholland Drive and Beverly Glen Boulevard. The open circles indicate locations of extensive damage or collapse of freeway structures: 1—Gavin Canyon undercrossing; 2—Interstate 5 and SR14 interchange; 3—Mission Gothic undercrossing of SR118; 4—Bull Creek Canyon Channel bridge; 5—La Cienega–Venice undercrossing of Interstate 10; and 6—Fairfax-Washington undercrossing of Interstate 10. Smoothed contours of horizontal peak ground velocity are shown by heavy dashed and full lines (Trifunac et al. 1996). This figure is included as a general background.

Trifunac and Todorovska (1997a,b) divided the study areas in blocks of 1×1 km^2 and counted the number of red-tagged buildings, N, and breaks in water pipes, n, in each block. This discretization acted as a filter, smoothing variations in the total stock of buildings and water pipe lines per km^2. Fig. 1 shows an overlay of areas with $N > 5$ (hatched) and $n > 6$ (densely

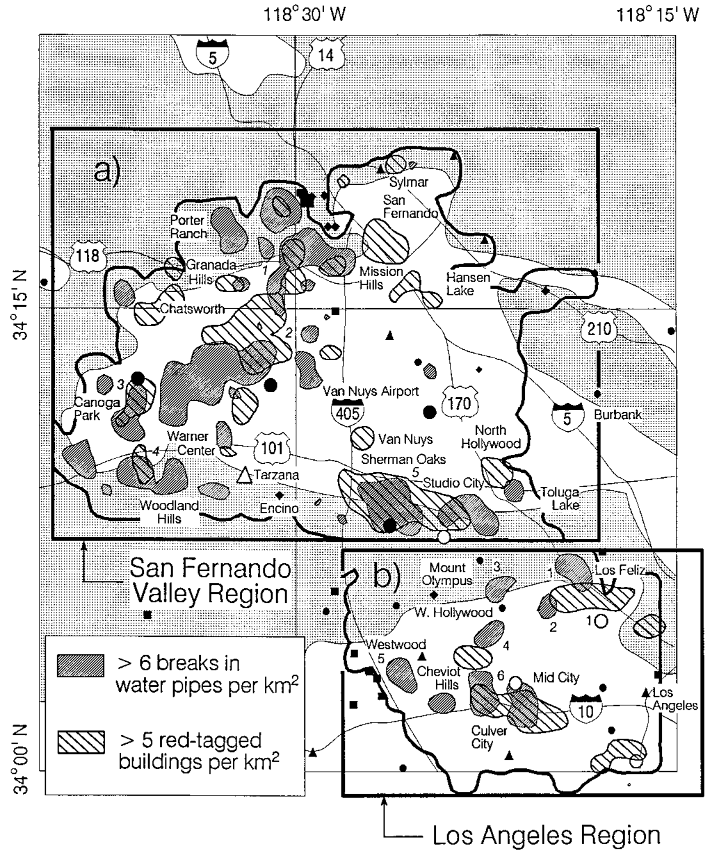

FIG. 1. Areas in (a) San Fernando Valley and (b) Los Angeles Where More Than 6 Breaks in Water Pipes and More Than 5 Red-Tagged Buildings Were Observed per km^2, during Northridge Earthquake

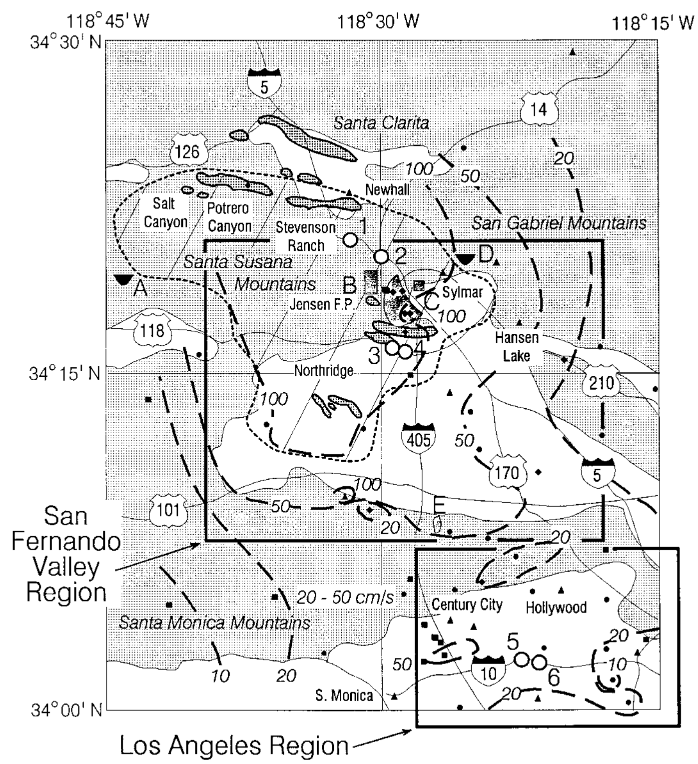

FIG. 2. Epicentral Area of Northridge Earthquake (M_L = 6.4), with Surface Projection of Ruptured Area (- - -), Contours of Peak Horizontal Ground Velocity (in cm/s, – – – and ——), Zones of Concentrated Ground Breakage (Shaded Regions Outlined by Heavy Solid Lines), and Locations of Extensive Damage or Collapse of Freeway Structures (○)

shaded). It is seen that the areas with $N > 5$ and $n > 6$ overlap at selected locations (e.g., in Sherman Oaks, at several locations in Northridge, Reseda, and Canoga Park, and along Interstate 10 in Los Angeles), but at many other locations there is very little overlap (Trifunac and Todorovska 1997c, 1998a). Density of pipe breaks $n > 6$ per km^2 indicates some form of nonlinear soil response (Trifunac and Todorovska 1996, 1997b). Therefore, nonlinear soil response may have decreased the damage to structures in some areas by absorbing the energy of shaking.

The peak horizontal strain, ε, near the ground surface can be related to the peak horizontal ground velocity, v_{max}, and to the average shear wave velocity in the 30 m soil layer at the surface, $\bar{v}_s$ (Trifunac and Lee 1996). It can be approximated by $\varepsilon = Av_{max}/\bar{v}_s$, where A is a function which depends on the relative location of the source and the site, the depth of the source, the regional geology, and the near surface geology at the site. Synthetic ground motion in parallel layers and also strain data recorded in Japan (Trifunac and Lee 1996) show that A is between 0.4 and 1.5. Trifunac et al. (1996) termed the ratio $v_{max}/\bar{v}_s$ as "strain factor" and drew smoothed contour maps for $v_{max}/\bar{v}_s$ for the Northridge earthquake, based on recorded peak ground velocities and measured $\bar{v}_s$ at the strong motion sites.

Maps of the physical properties of quaternary sedimentary deposits in San Fernando Valley by Tinsley and Fumal (1985) show that the western part of the valley has mostly fine and medium grained Holocene deposits, with shear wave velocity $v_s < 285$ m/s. The eastern part of the valley (east of Woodman Avenue) is covered by coarse and very coarse grained Holocene deposits and by fine and medium grained Pleistocene deposits, which have shear wave velocities in the range of 330 to 830 m/s. Ideally, these maps should be used to estimate the ground strain during strong earthquake shaking, but ground velocity during the Northridge earthquake was measured only at selected (unequally spaced) sites. In their analysis of density of water pipe breaks, n, as function of the ground strain, $\varepsilon = Av_{max}/\bar{v}_s$, Trifunac and Todorovska (1997b) assumed $A = 1$ and used the smooth contour maps of $v_{max}/\bar{v}_s$ from Trifunac et al. (1996), to assign ε to the 1×1 km^2 blocks where n was measured. Considering all the other assumptions in their work as well as in the study in this paper (e.g., uniform density and earthquake resistance of pipes and houses in the areas studies), to assume $A = 1$ is reasonable.

Trifunac and Todorovska (1997b) arrived at the following relationship between the average value of n, $\bar{n}$ (per km^2), and ε:

$$\log_{10}\bar{n} = \begin{cases} 1.60 + 0.464 \log_{10}\varepsilon & \text{for } -3.50 \le \log_{10}\varepsilon - 2.35 \\ 4.216 + 1.579 \log_{10}\varepsilon & \text{for } -2.35 \le \log_{10}\varepsilon < -2.0 \end{cases} \tag{1}$$

which is shown in Fig. 3 along with the data points (open circles). The vertical bars indicate the range of observed n in selected areas in San Fernando Valley and in Los Angeles. The numbering system for San Fernando Valley (1–5) and for Los Angeles (1–6) is consistent with that in Fig. 1. The areas in San Fernando Valley are 1—Granada Hills; 2—Northridge; 3—Canoga Park; 4—Woodland Hills; and 5—Sherman Oaks. In Los Angeles, numbers 1 through 6 correspond to 1—North of Freeway 101; 2—Highland Avenue; 3—Hollywood Hills; 4—La Cienega Blvd., 5—Motor Avenue; and 6—Santa Monica Freeway. The change of slope in Fig. 3 and in (1) at $\bar{n} \sim 3$ ($\log_{10}\varepsilon \gtrsim -2.3$) indicates that soil failure may have been initiated. In Fig. 1, the zones with $n \ge 6$ are shaded.

Field evidence (slope failures, ground cracking, compressive failures, tension breaks, vertical offsets across cracks formed by graben, etc.) in the areas with high density of pipe breaks supports the interpretation that nonlinear response of

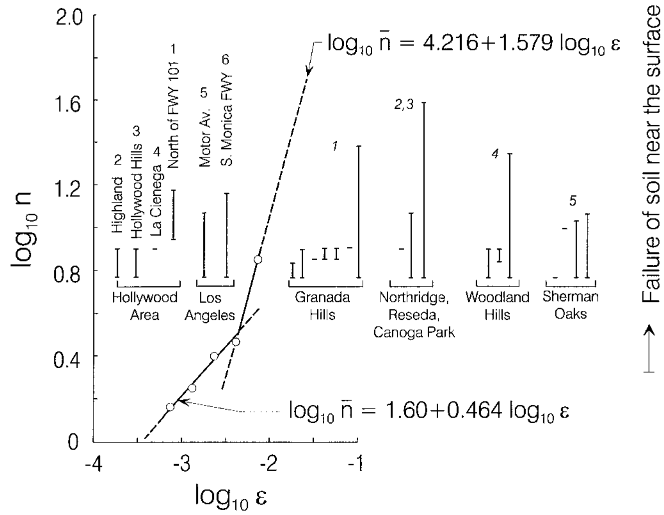

FIG. 3. Density of Breaks in Water Pipes, *n*, versus Strain Factor, ε (Redrawn from Trifunac and Todorovska 1997b)

soil did occur (Stewart et al. 1994; Holzer et al. 1996). Another indicator of nonlinear soil response is the reduction of peak horizontal acceleration, a_{max}, at "soft" soil sites ($\bar{v}_s < 360$ m/s) relative to the average trend at "hard" soil sites ($v_s > 360$ m/s), for strain factors $\log_{10}\varepsilon \gtrsim -2.5$. The onset of this decrease in recorded peak accelerations could be noticed even for $\log_{10}\varepsilon = -3.0$. This suggests that $n \gtrsim 2$ per km^2 may indicate the onset of nonlinear site response when $\bar{v}_s < 360$ m/s. In Fig. 1, the enlarged open and full station symbols indicate, respectively, larger and smaller recorded peak horizontal acceleration, relative to the average trend at "hard" soil sites, as reported by Trifunac and Todorovska (1996).

ANALYSIS

Density of Red-Tagged Buildings as Function of v_{max} or I_{MM} and Ground Strain

The two areas studied, San Fernando Valley and Los Angeles, were divided into 1×1 km^2 blocks. In each block, the number of red-tagged buildings, N, and the number of breaks in water pipes were counted. Also each block was assigned a value of horizontal peak ground velocity, v_{max}, and intensity of shaking, I_{MM}, using the smoothed contour maps in Trifunac et al. (1996) and in Dewey et al. (1994).

Then the average of N, $\bar{N}$, was calculated over selected intervals of n and v_{max} (Table 1), and of n and I_{MM} (Table 2). The intervals for n were "O" for $n = 0$; "A" for $1 \le n \le 4$; "B" for $5 \le n \le 9$; "C" for $10 \le n \le 14$; "D" for $15 \le n \le 19$.; "E" for $20 \le n \le 24$; and "F" for $25 \le n \le 29$, but the data was marginally sufficient to consider only the intervals O–C. The intervals for v_{max} were $10 \le v_{max} < 20$ cm/s; $20 \le v_{max} \le 50$ cm/s; $50 \le v_{max} < 100$ cm/s; $100 \le v_{max} < 150$ cm/s; and $v_{max} \ge 150$ cm/s (Table 1). Data was available for intensity levels I_{MM} = VI, VII, VIII, and IX (Table 2).

Based on the data in Table 1, in Fig. 4(a), v_{max} is plotted versus $\log_{10}\bar{N}$ for the ranges of n where data was available (for classes "O"–"E," the weak lines). The open circles show $\log_{10}\bar{N}$, averaged over all intervals of n, and the heavy line shows the corresponding linear fit

$$\log_{10}\bar{N} = (v_{max} - 64)/94 \tag{2}$$

(where explicit dependence on n was not considered) [Trifunac and Todorovska 1997(a)]. Fig. 4(b) is a similar presentation of the data on N as a function of intensity of shaking. The weak lines show I_{MM} versus $\log_{10}\bar{N}$ for different ranges of n

TABLE 1. Average Number of Red-Tagged Buildings, $\bar{N}$, per km^2, versus Peak Velocity of Strong Motion, v_{max}, and Number of Breaks in Water Pipes, n, in Same 1 km^2 Area

	PEAK STRONG MOTION VELOCITY, v_{max}									
	10–20 cm/s		20–50 cm/s		50–100 cm/s		100–150 cm/s		>150 cm/s	
Range of n (1)	Data points (2)	$\bar{N}$ (3)	Data points (4)	$\bar{N}$ (5)	Data points (6)	$\bar{N}$ (7)	Data points (8)	$\bar{N}$ (9)	Data points (10)	$\bar{N}$ (11)
O (0)	22	0.14	109	0.72	73	0.95	32	4.66	—	—
A (1–4)	9	0.11	114	0.48	109	1.41	61	2.90	5	11.40
B (5–9)	—	—	30	0.97	19	2.16	30	5.37	8	11.75
C (10–14)	—	—	4	1.25	4	2.75	9	3.44	4	12.00
D (15–19)	—	—	—	—	—	—	6	5.17	—	—
E (20–24)	—	—	—	—	(1)	(5.00)	4	4.50	—	—

TABLE 2. Average Number of Red-Tagged Buildings, $\bar{N}$, per km^2, versus Site Intensity, I_{MM}, and Number of Breaks in Water Pipes, n, in Same 1 km^2 Area

	MODIFIED MERCALLI INTENSITY, I_{MM}							
	I_{MM} = VI		I_{MM} = VII		I_{MM} = VIII		I_{MM} = IX	
Range of n (1)	Data points (2)	$\bar{N}$ (3)	Data points (4)	$\bar{N}$ (5)	Data points (6)	$\bar{N}$ (7)	Data points (8)	$\bar{N}$ (9)
O (0)	9	0.00	178	0.62	46	2.50	7	10.71
A (1–4)	5	0.40	137	0.53	140	1.78	16	7.50
B (5–9)	—	—	21	0.71	36	1.53	31	8.23
C (10–14)	—	—	(1)	(1.00)	3	1.67	17	5.24
D (15–19)	—	—	—	—	—	—	7	4.43
E (20–24)	—	—	—	—	—	—	5	4.60

(see Table 2); the open circles show $\log_{10}\bar{N}$, averaged over all intervals of n; and the heavy line shows the corresponding fit

$$\log_{10}N = -0.876 - 0.117I_{MM} + 0.033I_{MM}^2 \tag{3}$$

from Trifunac and Todorovska [1997(a)].

Observing the trends of $\log_{10}\bar{N}$ versus v_{max} or I_{MM} in Figs. 4(a,b), it is seen that, in the range $35 \lesssim v_{max} \lesssim 125$ cm/s and VII $\leq I_{MM} \leq$ VIII, for progressively larger values of n, $\log_{10}\bar{N}$ grows slower with increasing v_{max} or I_{MM}. For $v_{max} \gtrsim 125$ cm/s and $I_{MM} >$ VIII, the slope of $\log_{10}\bar{N}$ versus v_{max} and I_{MM} becomes similar for all n.

In Table 1 and in Fig. 4(a), for $n = 0$ and for $20 \leq v_{max} < 50$ cm/s (109 data points, $\bar{N} = 0.72$), the trend of $\log_{10}\bar{N}$ versus v_{max} seems to contradict our interpretation. Ignoring this data point and considering the other average values of N for $n = 0$ (in the first row of Table 1) would result in the linear trend

$$\log_{10}\bar{N} = v_{max}/75 - 1 \tag{4}$$

Next, we describe the observed trends in Figs. 4(a,b) by simple analytical functions $N = f(v_{max}, n)$ and $N = f(I_{MM}, n)$. As the number of data points is not sufficient to perform a formal regression analysis, functions that approximately describe the observed trends were found by assuming a ‘‘reasonable’’ functional form, in which the parameters were selected by repeated trials. Candidates for these functions are presented in Figs. 5(a,b), respectively, for $N = f(v_{max}, n)$ and $N = f(I_{MM}, n)$. (From now on, it is understood that these functions refer to the average trends, and the bar over N is omitted.)

The analytical form for the functions in Fig. 5(a) is

$$\log_{10}N = \left(\frac{v_{max}}{s} - 1\right)\left(1 + \frac{a}{v_{max}^2}\right) + B(n)\,\frac{v_{max}}{v_p}\,e^{1 - v_{max}/v_p} \tag{5a}$$

where

$$s = \begin{cases} 85 & n > 2 \\ 80 & n \leq 2 \\ 75 & n \leq 1 \end{cases} \tag{5b}$$

$$a = 100 \tag{5c}$$

$$B(n) = \begin{cases} 0.25 + 0.04n & n > 0 \\ 0.5 & n = 0 \end{cases} \tag{5d}$$

and

$$v_p = \begin{cases} 35 & n > 0 \\ 15 & n = 0 \end{cases} \tag{5e}$$

In the analysis, values n = 2.5, 7, 12, 17, and 22 were taken, respectively, to represent the A, B, C, D, and E intervals. The term $(1 + a/v_{max}^2)$ has been adopted to ‘‘filter out’’ small values of v_{max} so that the resulting curves approach large negative values of $\log_{10}N$ as $N \to 0$. For $\log_{10}N > 0$ ($N > 1$), (5a) gives essentially the same results as (4) for computation of v_{max} from $\log_{10}N$. The unexplained value of $N = 0.72$ for $20 \leq v_{max} < 50$ m/s does not come into play, because one needs to use inverse of (5a) only for $N \geq 1$.

The expression for the functions in Fig. 5(b) is

$$\log_{10}N = \begin{cases} [b_0(n) + b_1(n)I_{MM} + b_2(n)I_{MM}^2]\left(1 + \dfrac{CI}{I_{MM}^3}\right); \\ \quad I_{MM} \geq I_{max} \\ (SI_{MM} - 3)\left(1 + \dfrac{CI}{I_{MM}^3}\right); \quad I_{MM} < I_{max} \end{cases} \tag{6a}$$

where

$$I_{max} = \begin{cases} 8 & n > 12.5 \\ 7 & 2.5 < n \leq 12.5 \\ 6 & n \leq 2.5 \end{cases} \tag{6b}$$

$$S = (b_0(n) + b_1(n)I_{max} + b_2(n)I_{max}^2 + 3)/I_{max} \tag{6c}$$

and

$$\left.\begin{aligned} b_0(n) &= -2.22 \\ b_1(n) &= 0.0263 \\ b_2(n) &= 0.0374 \end{aligned}\right\}; \quad n = 0 \tag{6d}$$

$$\left.\begin{aligned} b_0(n) &= -0.136 + 0.326n \\ b_1(n) &= -0.451 - 0.0688n \\ b_2(n) &= 0.0629 + 0.00342n \end{aligned}\right\}; \quad 0 < n < 27 \tag{6e}$$

$$\left.\begin{aligned} b_0(n) &= b_0(27) \\ b_1(n) &= b_1(27) \\ b_2(n) &= b_2(27) \end{aligned}\right\}; \quad n \geq 27 \tag{6f}$$

In (6a), the term $(1 + CI/I_{MM}^3)$ forces $\log_{10}N$ to approach large negative values for $I_{MM} \to 0$, since $\log N \to -\infty$ when $N \to 0$, for $I_{MM} \to 0$. Value of $CI = 6$ is taken in this analysis.

Inferences on v_{max} and I_{MM} from Data on n and N

Eqs. (5a) and (6a) can be inverted to compute v_{max} and I_{MM} for those 1 × 1 km^2 areas where both n and N are known.

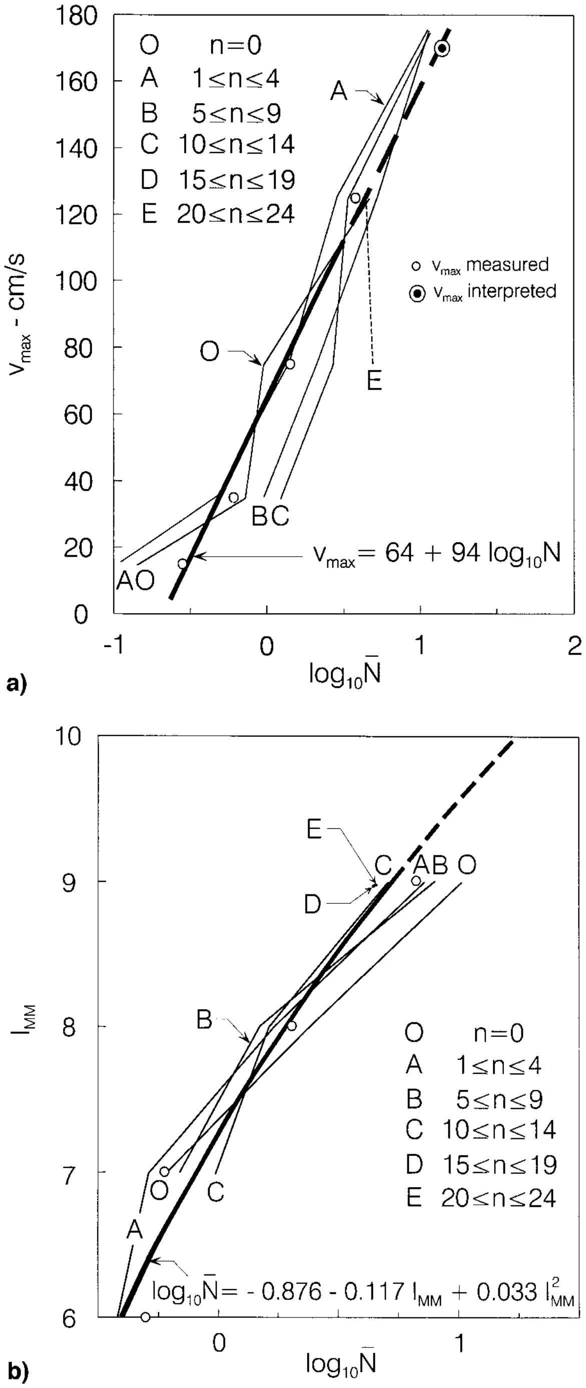

FIG. 4. (a) Peak Horizontal Ground Velocity, v_{max}, versus Average Observed Density of Red-Tagged Buildings, $\bar{N}$ per km^2, for Several Intervals of Density of Breaks in Water Pipes, n per km^2, in Range of 0–24 [O, A, B, C, D, and E (see Table 1)]; (b) Modified Mercalli Intensity, I_{MM}, versus Average Observed Density of Red-Tagged Buildings, $\bar{N}$ per km^2, also for Several Intervals, in Same Range (see Table 2)

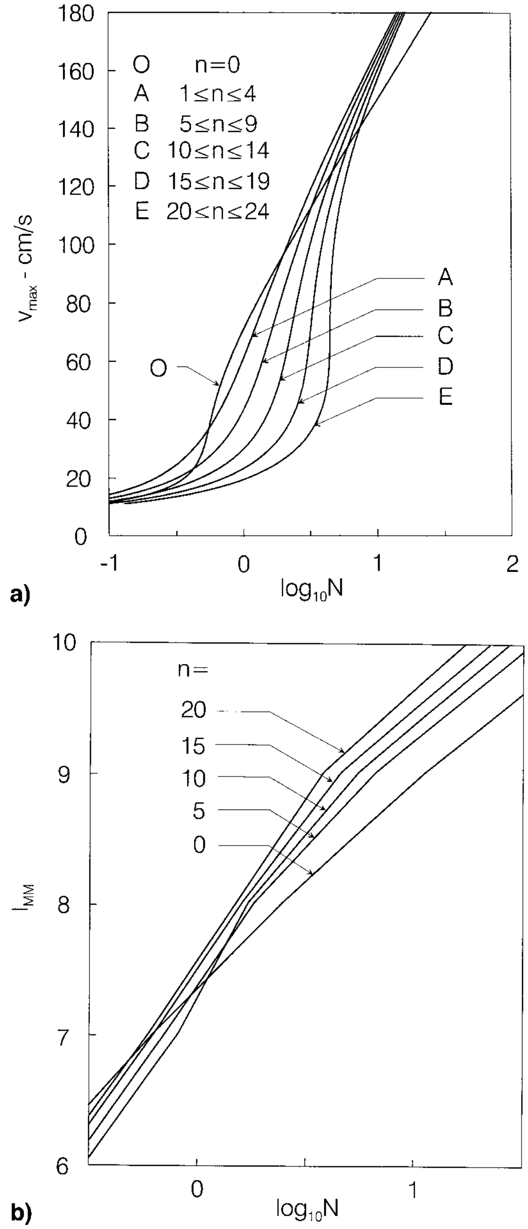

FIG. 5. Approximate Functional Dependence for (a) $\log_{10}N = f(v_{max}, n)$, Defined by (5*a*); and (*b*) $\log_{10}N = f(I_{MM}, n)$, Defined by (6*a*)

This will be possible only for $v_{max} \gtrsim 20$ cm/s and for $I_{MM} \gtrsim 7$, that is when $N \geq 1$.

To study possible departures from the ''smoothed'' maps of v_{max} (shown in Fig. 2), and I_{MM} (Dewey et al. 1994), the ''new'' estimates of v_{max} and I_{MM} were calculated for all 1 km^2 blocks with $N \geq 1$ and $n \geq 0$. For sites with $N = 0$, the original estimates of v_{max} and I_{MM} were kept. For both San Fernando Valley and Los Angeles areas, the overall trends of v_{max} and of I_{MM}, in Figs. 6 and 7, are consistent with those in Fig. 2 and in Dewey (1995). The updated estimates are increased or decreased only locally, when $N \geq 1$.

Fig. 6 suggests that $v_{max} > 150$ cm/s in San Fernando, Northridge [2 in Fig. 1(a)], Canoga Park [3 in Fig. 1(a)], Sherman Oaks [5 in Fig. 1(a)], along Sunset Boulevard, and along Santa Monica Freeway [2 and 6 in Fig. 1(b)]. Fig. 7 suggests that site intensity X was reached just west of Rinaldi receiving station in Granada Hills area [1 in Fig. 1(a)], south of station USC No. 53 [the full large circle near 3 in Fig. 1(a)] in Canoga Park, and in Sherman Oaks area [north of station USC No. 13, the full large circle near 5 in Fig. 1(a)], all in the San Fernando Valley area. It appears that intensity X was also reached along Sunset Boulevard in Hollywood [1 and 2 in Fig. 1(b)] and along Santa Monica Freeway near La Brea Avenue [6 in Fig. 1(b)]. The published map of site intensities, by Dewey et al. (1994), shows highest intensity I_{MM} = IX.

The maps of v_{max} and I_{MM} in Figs. 6 and 7 are ''approximate'' since these are results of only one cycle of iteration. We started with ''smooth'' v_{max} (Fig. 2) and I_{MM} [Dewey et al.

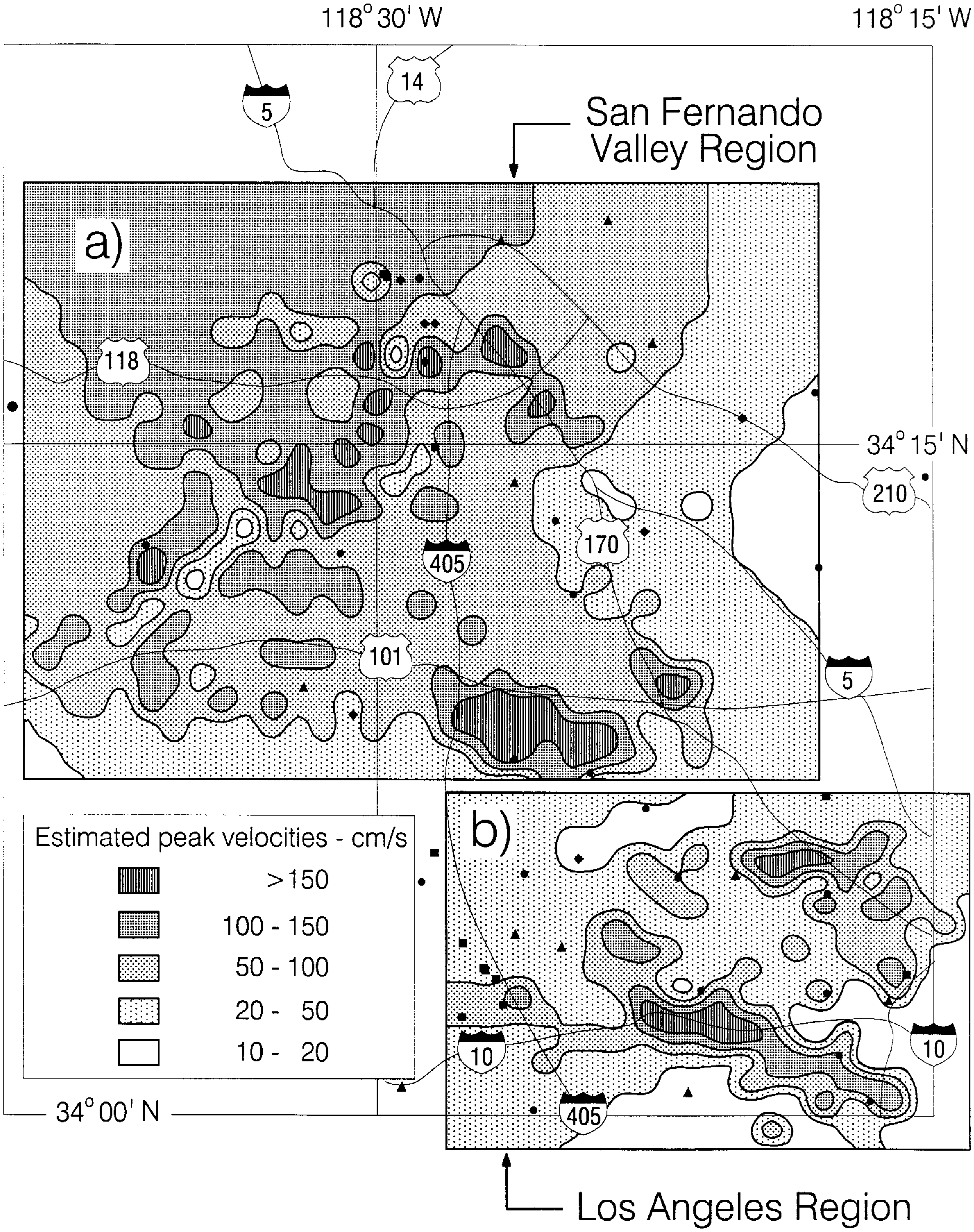

FIG. 6. Estimated Peak Velocities in San Fernando Valley and Los Angeles, Inferred from Observed Density of Red-Tagged Buildings, *N*, and Density of Breaks in Water Pipes, *n*, via Inverse of (5*a*)

1994), established approximate relationship between N, n, $v_{\max}$, and I_{MM}, and updated $v_{\max}$ and I_{MM} from observed n and N. We chose not to perform subsequent iteration steps because the number of stations which did record $v_{\max} \gtrsim 100$ cm/s is small (see Fig. 2), and we had no stations recording strong motion where n or N were large (Fig. 1) to evaluate independently the accuracy of this approach.

DISCUSSION

Did Nonlinear Soil Response Reduce Damage of Buildings?

The presented results [Fig. 4(a)] show that, for $35 \lesssim v_{\max} \lesssim 125$ cm/s, the rate of growth of $\log_{10}\underline{N}$ versus $v_{\max}$ becomes slower with increasing n. Our interpretation is that, in the early

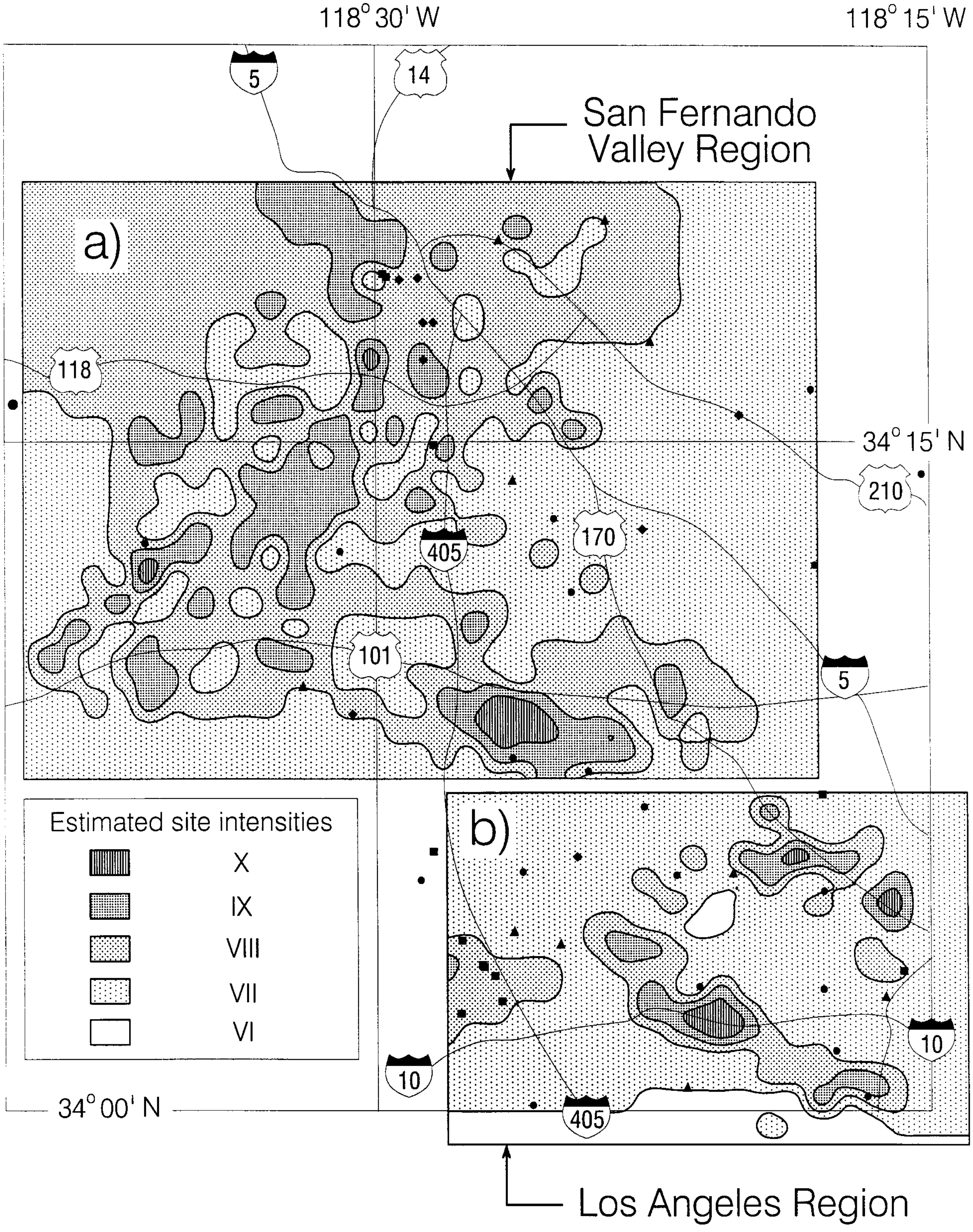

FIG. 7. Estimated Modified Mercalli Intensity in San Fernando Valley and Los Angeles Inferred from Observed Density of Red-Tagged Buildings, *N*, and Density of Water Pipe Breaks, *n*, via Inverse of (6*a*)

stages of nonlinear response of surface soils, say for $\varepsilon < 10^{-2.5}$, a part of the incident wave energy is absorbed, thus reducing the energy available for excitation and damage of structures. For larger strains (say $\varepsilon > 10^{-2.25}$), the soil fails, and large differential and nonlinear motions in the soil damage buildings and other structures via large deformation of the foundations, in addition to the already large inertial forces. Beyond v_{max} $\sim$150 cm/s and for strains $\varepsilon \gtrsim 10^{-2.5}$, the slope of $\log_{10}N$ seems to be less dependent on n and steeper than for $35 \lesssim v_{max} \lesssim 125$ cm/s [Fig. 4(a)].

For larger building plan dimensions, the degree of damage to low rise residential structures is expected to increase because of larger differential motions (Trifunac 1997; Trifunac and Todorovska 1997d). As reported by the U.S. Department of Housing and Urban Development (1994), of all single family detached units (small plan dimensions), 2% were red-tagged. Of single family attached buildings, 3% were red-tagged, and of low-rise multifamily buildings (the largest plan dimensions), 6% were red-tagged. Case studies of 54 single family detached buildings, which experienced severe damage during the Northridge earthquake, had low incidence of structural damage. The most common sources of damage were related to fissures and settlement of the ground. This statistic is consistent with our interpretation of the simultaneous action of shaking and of differential motions on the damage of the SFD structures in the area.

More than 65% of the area studied in this paper (65% in San Fernando Valley and 67% in Los Angeles) experienced $v_{\max}$ between 20 and 100 cm/s and thus may have experienced some degree of absorption of incident wave energy by nonlinear soil response. The scatter of the observed data is considerable, but it appears that the first noticeable indications of nonlinear soil response. in the amplitudes of recorded horizontal peak accelerations, may occur near $\log_{10}(v_{\max}/\bar{v}_s) \sim -3.0$, and may become pronounced for $\log_{10}(v_{\max}/\bar{v}_s) \sim -2.5$ (Trifunac and Todorovska 1996). Less than 4% of the areas studied in this paper (4% for San Fernando valley and 2% for Los Angeles) appear to have experienced $v_{\max} > 150$ cm/s. There, large densities of breaks in water pipes and of red-tagged buildings resulted from various types and degrees of soil failure and from large inertial forces combined.

Spatial Variations of Strong Ground Motion

The geographical distribution and the patterns of high and of low peak velocities of strong motion (Fig. 6) and of variations of estimated site intensity (Fig. 7) do not coincide with the simple site characteristics which have been mapped so far, (e.g., Holocene deposits, depth to ground water, and liquefaction susceptibility (see Tinsley et al. 1985; Trifunac and Todorovska 1997a,b; 1998a,b). Yet, recorded strong motion data, e.g., in Tarzana and Santa Monica (Spudich et al. 1996; Gao et al. 1996) and the results in this paper imply existence of ''small'' regions, with dimensions of one to several kilometers, where the amplitudes of strong motion can be at least several times larger than in the neighboring areas, and other non-overlapping zones of comparable dimensions where the strain exceeded the average strain levels in the area. At sites where the near surface soil responded linearly the observed amplification of strong motion may be explained by focusing and interference of incident waves (Gao et al. 1996; Spudich et al. 1996). The locations on the ground surface where the focusing and interference of seismic waves increase or decrease the amplitudes of the incident waves depend on the angle of the arriving waves and on the geometry of the sediments and of the soil deposits (Trifunac 1971; Todorovska and Trifunac 1997a,b). Thus, from elastic wave propagation and interference point of view, the areas experiencing high amplification would be different during different earthquakes (the strong motion site in Tarzana may be an exception). The geographical distribution of strong motion amplitudes is further complicated by nonlinear response of soils, which reduces the strong motion energy of shaking arriving to the surface of the site. Large surface strains do occur in the areas of strong shaking, but frequently do not coincide with the areas where N is large (Trifunac and Todorovska 1997c, 1998a). The causes for this nonlinear response of soils must be sought in geotechnical characteristics of the site. At present it is not possible to predict the location of nonlinear response of soils during future earthquakes nor the mechanism that may cause these sites to be reactivated or to migrate during future earthquakes (Trifunac and Todorovska 1998a,b). The large alluvial slide caused by the 1971 San Fernando earthquake (extending from Juvenile Hall in San Fernando Valley towards southwest and towards Van Norman Lake) was reactivated and possibly enlarged by the 1994 Northridge earthquake, indicating that the size of the slide mobilized may depend also on the earthquake characteristics. For the majority of sites experiencing soil failure during the Northridge earthquake, it is not known whether those may have moved during some previous earthquakes. Obviously, the above are important considerations which should be understood prior to future work attempting to map the related hazard parameters for use in earthquake resistant design (Todorovska 1995; Todorovska and Trifunac 1996, 1998).

To understand and to explain the above interpretation implying rapid fluctuations of $v_{\max}$ and of I_{MM} (caused by seemingly random occurrence of areas with ''linear'' site amplification and elsewhere by ''nonlinear'' soil response), very dense arrays of strong motion recorders (perhaps 1 instrument per km^2) must be deployed and maintained for many years. Also, very detailed geotechnical and geological site investigations will be required to identify the causes and the extent of linear as well as of nonlinear soil response. Those site investigations should be carried out soon after all well-documented earthquakes.

The modified Mercalli intensity map (Dewey et al. 1994) for the Northridge earthquake was based on some 130 sampled sites in the greater Los Angeles area, but the contours for $I_{MM} \geq 8$ were based on only 31 points. It is possible (Lekkas 1996) and it would be useful to increase the density of the observation points significantly, especially in the heavily shaken areas (say for $I_{MM} \geq 7$).

The installation of strong motion arrays worldwide has been guided by many diverse engineering and seismological goals. To speed up data accumulation, arrays have been deployed where earthquakes were expected to occur, and often far from populated areas. The lessons from the Northridge earthquake show that, to advance earthquake engineering, motions in and around man made structures must be studied first and in detail, as well as motions of soils and of geological strata typical of the areas covered by large cities, even if this requires long waiting periods before useful data is recorded (Trifunac 1988; Trifunac et al. 1994). Deterministic and in-depth studies of the earthquake source are useful for advancement of knowledge about the mechanics of earthquake energy release (Trifunac 1974; Wald et al. 1996). However, unless propagation, focusing, and local effects are understood also and properly taken into consideration, it will be difficult to improve the rational basis for selection of design ground motions.

CONCLUSIONS

The data on red-tagged buildings and breaks in water pipes in typical residential areas of San Fernando Valley and Los Angeles were analyzed to explore their mutual dependence. The ground shaking was characterized by the horizontal peak ground velocity, $v_{\max}$, and by the modified Mercalli intensity, I_{MM}. Functional relationships were derived for the dependence of the density of red-tagged buildings per km^2, N, on the amplitude of ground shaking ($v_{\max}$ or I_{MM}) and on the ground strain, measured by the density of breaks in water pipes per km^2, n (large n indicates large ground strain). Our interpretation of the observed trends is that the number of severely damaged buildings was reduced in areas where the surface soil experienced some form of nonlinear response (say for $\varepsilon < 10^{-2.5}$), because the soil absorbs part of the incident wave energy. In the areas where the strains in the soil were very large (say $\varepsilon > 10^{-2.25}$), or where the soil failed (slope failures, ground cracking, compressive failures, tension cracks, vertical offsets formed by graben, etc.), large differential ground motions took place and deformed the building foundations, resulting in pseudo static damage of the buildings in addition to the damage caused by large inertial forces. This negative effect of large ground strains should be more significant for larger in plan buildings.

The functional relationships $N(v_{max}, n)$ and $N(I_{MM}, n)$ were inverted to obtain v_{max} and I_{MM} from observed N and n. The inverse functions were used to estimate spatial distribution of v_{max} and I_{MM} in the regions studied (under the assumptions that the distribution of buildings and water pipes in typical residential areas of these two regions is approximately uniform). The results suggest variation of ground motion within distances of only a few kilometers. These variations could not be measured with the current density of (1) strong motion stations and (2) sites where reports on felt intensity of shaking were gathered. The ''smooth'' appearance of the modified Mercalli intensity map and of the contour maps of peak amplitudes of strong motion (e.g., Fig. 2), in epicentral areas, therefore could be the consequence of too sparse spatial sampling, and may not reflect the spatial variation of strong motion amplitudes with adequate resolution.

Contour maps of peak acceleration, velocity, and displacement, of the polarity of peak amplitudes (Todorovska and Trifunac 1977b), and of Pseudo Relative Velocity (PSV) spectral amplitudes (Todorovska and Trifunac 1997a), suggest slowly changing peak amplitudes, with the same polarity over distances that often exceed the separation distances between adjacent recording stations, and for epicentral distances greater than 30 to 40 km. In contrast, Figs. 6 and 7 and the analysis in this paper suggest more rapid and complex fluctuation of strong motion amplitudes. These fluctuations appear to be caused by an irregular and little understood mosaic of soil responses to strong shaking, oscillating from ''linear'' to ''nonlinear'' zones (Trifunac and Todorovska 1997c; 1998a,b). The challenge for future research is to measure, understand, and interpret these fluctuations. If it can be shown that these zones are related to some specific site characteristics, so that nonlinear response will be repeated during future earthquakes, the ability of soil layers to absorb incident wave energy can be used as a passive isolation system in future innovative and advanced design applications.

APPENDIX. REFERENCES

Dewey, J. W., Reagor, B. G., and Dengler, L. (1995). ''Isoseismol map of the Northridge, California, earthquake of January 17, 1994.'' *Earthquake Spectra*, 11, Supplement C, Vol. 1.

Earthquake Engineering Research Institute (1994). ''Northridge earthquake, January 17, 1994, preliminary reconnaissance report.'' *EERI 94-01*, Oakland, Calif.

Earthquake Engineering Research Institute (1996). ''Northridge earthquake renaissance report.'' *Earthquake Spectra*, 11, Supplement C, Vol. 1, 2.

Gao, S., Liu, H., Davis, P. M., and Knopoff, L. (1996). ''Localized amplification of seismic waves and correlation with damage due to Northridge earthquake: Evidence for focusing in Santa Monica.'' *Bull. Seismological Soc. of Am.*, 26(1B), S209–S230.

Harp, E. L., and Jibson, R. W. (1966). ''Landslides triggered by 1994 Northridge, California, earthquake.'' *Bull. Seismological Soc. of Am.*, 86(1B), S319–S332.

Holzer, T. L., Bennett, M. J., Tinsley, J. C., Ponti, D. J., and Sharp, R. V. (1996). ''Causes of ground failure in alluvium during the Northridge, California, earthquake of January 17, 1994.'' *Proc., 6th U.S.-Japan Workshop on Earthquake Resistant Design of Lifeline Facilities and Counter Measures for Soil Liquefaction*, Tokyo, Japan.

Kanai, K. (1983). *Engineering Seismology*. Univ. of Tokyo Press.

Lekkas, E. L. (1996). ''Pyrgos earthquake damages (based on E.M.S.-1992) in relation with geological and geotechnical conditions.'' *Soil Dyn. and Earthquake Engrg.*, 15(2), 61–68.

Spudich, P., Hellweg, M., and Lee, W. H. K. (1996). ''Directional topographic response at Tarzana observed in aftershocks of the 1994 Northridge, California earthquake: Implication for main shock motion.'' *Bull. Seismological Soc. of Am.*, 80(1B), S193–S208.

Stewart, J. P., Bray, J. D., Seed, R. B., and Sitar, N. (1994). ''Preliminary report on the principal geotechnical aspects of the January 17, 1994, Northridge earthquake.'' *Rep. No. UCB/EERC-94/08*, University of California, Berkeley, Calif.

Tinsley, J. S., and Fumal, T. E. (1985). ''Mapping quaternary sedimentary deposits for areal variations in shaking response,'' in ''Evaluating earthquake hazards in the Los Angeles region,'' J. I. Ziony, ed. *U.S. Geological Survey Professional Paper (1360)*, Washington, D.C., 101–125.

Tinsley, J. C., Youd, J. L., Perkins, D. M., and Chen, A. T. F. (1985). ''Evaluating liquefaction potential,'' in ''Evaluating earthquake hazards in the Los Angeles region,'' J. I. Ziony, ed. *U.S. Geological Survey Professional Paper (1300)*, Washington, D.C., 263–316.

Todorovska, M. I. (1995). ''Uniform probability response spectra for selecting site specific design motions.'' *Proc. 3rd Int. Conf. on Recent Advances in Geotech. Earthquake Engrg. and Soil Dyn.*, St. Louis, Mo., 2, 613–618.

Todorovska, M. I., and Trifunac, M. D. (1996). ''Hazard mapping of normalized peak strain in soil during earthquakes: Microzonation of a metropolitan area.'' *Soil Dyn. and Earthquake Engrg.*, 15(5), 321–329.

Todorovska, M. I., and Trifunac, M. D. (1997a). ''Distribution of pseudo spectral velocity during the Northridge, California, earthquake of 17 January, 1994.'' *Soil Dyn. and Earthquake Engrg.*, 16(3), 173–192.

Todorovska, M. I., and Trifunac, M. D. (1997b). ''Amplitudes, polarity and time of peaks of strong ground motion during the 1994 Northridge, California, Earthquake.'' *Soil Dyn. and Earthquake Engrg.*, 16(4), 235–258.

Todorovska, M. I., and Trifunac, M. D. (1998). ''Discussion of 'The role of earthquake hazard maps in loss estimation: A study of the Northridge earthquake.' '' *Earthquake Spectra*, 14(3), 557–563.

Trifunac, M. D. (1971). ''Surface motion of a semi-cylindrical alluvial valley for incident plane SH waves.'' *Bull. Seismological Soc. of Am.*, 61, 1755–1770.

Trifunac, M. D. (1974). ''A three-dimensional dislocation model for the San Fernando, California, earthquake of February 9, 1971.'' *Bull. Seismological Soc. of Am.*, 64, 149–172.

Trifunac, M. D. (1988). ''A note on peak accelerations during 1 and 4 October, 1987, earthquakes in Los Angeles, California.'' *Earthquake Spectra*, 4(1), 101–113.

Trifunac, M. D. (1997). ''Differential earthquake motion of building foundations.'' *J. Struct. Engrg.*, ASCE, 123(4), 414–422.

Trifunac, M. D., and Lee, V. W. (1996). ''Peak surface strains during strong earthquake motion.'' *Soil Dyn. and Earthquake Engrg.*, 15(5), 311–319.

Trifunac, M. D., and Todorovska, M. I. (1996). ''Nonlinear soil response—1994 Northridge, California, earthquake.'' *J. Geotech. Engrg.*, ASCE, 122(9), 725–735.

Trifunac, M. D., ad Todorovska, M. I. (1997a). ''Northridge, California, earthquake of 1994: Density of red-tagged buildings versus peak horizontal velocity and intensity of shaking.'' *Soil Dyn. and Earthquake Engrg.*, 16(3), 209–222.

Trifunac, M. D., and Todorovska, M. I. (1997b). ''Northridge, California, earthquake of 1994: Density of pipe breaks and surface strains.'' *Soil. Dyn. and Earthquake Engrg.*, 16(3), 193–207.

Trifunac, M. D., and Todorovska, M. I. (1997c). ''Closure to 'Nonlinear soil response: 1994 Northridge, California, earthquake.' '' *J. Geotech. Engrg.*, ASCE, 123(10), 988–989.

Trifunac, M. D., and Todorovska, M. I. (1997d). ''Response spectra and differential motion of columns.'' *Earthquake Engrg. and Struct. Dyn.*, 26(2), 251–268.

Trifunac, M. D., and Todorovska, M. I. (1998a). ''Nonlinear soil response as a passive isolation mechanism—the 1994 Northridge, California, earthquake.'' *Soil Dyn. and Earthquake Engrg.*, 17(1), 41–51.

Trifunac, M. D., and Todorovska, M. I. (1998b). ''Damage distribution during the 1994 Northridge, California, earthquake relative to generalized categories of surficial geology.'' *Soil Dyn. and Earthquake Engrg.*, 17(4), 239–253.

Trifunac, M. D., Todorovska, M. I., and Ivanović, S. S. (1994). ''A note on distribution of uncorrected peak ground accelerations during Northridge, California, earthquake of 17 January 1994.'' *Soil Dyn. and Earthquake Engrg.*, 13(3), 187–196.

Trifunac, M. D., Todorovska, M. I., and Ivanović, S. S. (1996). ''Peak velocities and peak surface strains during Northridge, California, earthquake of 17 January 1994.'' *Soil Dyn. and Earthquake Engrg.*, 15(5), 301–310.

U.S. Department of Housing and Urban Development (1994). ''Assessment of damage to residential buildings caused by Northridge earthquake.'' *USDHUD Report*, HUD-1499-PDR, Washington, D.C.

Wald, D. J., Heaton, T. H., and Hudnut, K. W. (1996). ''The slip history of the 1994 Northridge, California, earthquake determined from strong motion, teleseismic, GPS, and leveling data.'' *Bull. Seismological Soc. of Am.*, 86(1B), S49–S70.